Single-Molecule Magnet Behavior in a Tb-Nitronyl Nitroxide Radical Network with [Tb 3 (NIT) 2] Nodes

Chao-Yi Jin, Xue-Lan Mei, Yan Zhou, Licun Li, Jean-Pascal Sutter

Single-Molecule Magnet Behavior in a Tb-Nitronyl Nitroxide Radical Network with [$Tb_3(NIT)_2$] Nodes

Chao-Yi Jin,[a] Xue-Lan Mei,[*b] Yan Zhou,[a] Licun Li[*a] and Jean-Pascal Sutter[*c]

[a] *Department of Chemistry, Key Laboratory of Advanced Energy Materials Chemistry, College of Chemistry, Nankai University, Tianjin 300071, China*
[b] *College of Materials Science and Chemical Engineering, Bengbu University, Bengbu, 233030, P. R. China*
[c] *Laboratoire de Chimie de Coordination du CNRS (LCC-CNRS), Université de Toulouse, CNRS, Toulouse, France*

ABSTRACT: Two rare two-dimensional Ln-radical networks, namely, [{$Ln(tfa)_3$}$_3$(NIT-4Py)$_2$]$_n$ [Ln^{III} = Gd **1** and Tb **2**; tfa^- = trifluoroacetylacetonato; NIT-4Py = 2-(4-pyridyl)-4,4,5,5-tetramethylimidazoline-1-oxyl-3-oxide] have been successfully constructed and characterized. In these complexes, each NIT-4Py radical functions as a tridentate ligand to ligate to three Ln ions, creating a 2D network with linear five-spin [$Ln_3(NIT)_2$] nodes. Ferromagnetic Ln-NO interactions govern the characteristic magnetic behavior of a finite spin system. The Tb complex is shown to exhibit SMM behavior in zero dc field with an energy barrier for spin flipping of 53 K and a hysteretic M-H behavior at 2.3 K with coercive field H_{coer} = 110 Oe. This complex represents the first example of a Ln-nitronyl nitroxide SMM-based network.

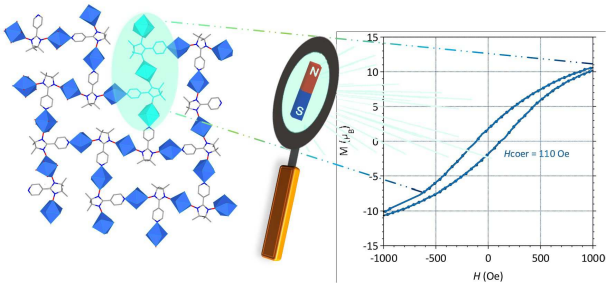

INTRODUCTION

Lanthanide single-molecule magnets (SMMs) have been a major topic in the field of molecular magnetism due to their appealing slow magnetic relaxation behaviors arising from the strong magnetic anisotropy of Ln ions.[1-7] Recently, significant progress towards high blocking temperatures and large coercive fields have been reported;[8-13] for instance, Layfield et al. presented a mononuclear Dy metallocene cation $[(Cp^{iPr5})Dy(Cp^*)]^+$ (Cp^{iPr5}: penta-iso-propylcyclopentadienyl; Cp*: pentamethylcyclopentadienyl) with the record magnetic blocking temperature 80 K as well as effective barrier of 1541 cm^{-1};[10] more recently, Long et al reported a mixed-valence binuclear Dy complex $(Cp^{iPr5})_2Dy_2I_3$ featuring metal-metal bonding which displays an enormous coercive magnetic field with a lower bound of 14 T at 60 K.[11]

Ideally, the relaxation of the magnetization for an SMM is controlled by an energy barrier and follows the Arrhenius behavior; it is known as the Orbach mechanism. However, in real systems, several processes are at work,[14] and one of the important contributions to the relaxation of the magnetization involves molecular vibrations. It was suggested that designing structurally more rigid SMM can reduce the under-barrier spin relaxation by phonon contributions.[15, 16] One straightforward possibility is to incorporate the SMM into an extended chemical network, which is inherently more rigid. In this context, Ln-SMMs can be used as magnetic building blocks to construct extended systems.[17-20] Following such an approach, the coordination geometries of Ln ions and magnetic exchanges can be controlled through rational structural design and crystal engineering, resulting in the appealing magnetic performance.[21-25] Moreover, for practical applications, SMMs imbedded in extended structures are expected to be better candidates than discrete molecules because the ordered arrangement of SMMs is essential for surface-based devices.[18, 26] Achieving organized arrays of molecular nanomagnets remains a main challenge.

SMMs combining 4f ions and organic radicals are attracting interest because the exchange coupling between the paramagnetic centers can result in a large ground spin

state and help to suppress QTM.[27-31] The metal-radical approach has been used to obtain the extended networks (2- and 3-D) behaving as magnets[32-38] but rather seldom to imbed Ln-Radical SMMs into extended networks. The most widely used radical unit is nitronyl nitroxide (hereinafter NIT), due to its chemical adaptability (functionalization), exceptional stability and versatility in coordination modes. NIT-Ln complexes are intriguing platforms for designing molecular nanomagnets exhibiting appealing magnetic relaxation behavior,[28, 39-48] but NIT-Ln SMM based network remains unexplored. Therefore, the possibility of achieving a Ln-radical SMM incorporated in a coordination framework has been considered herein.

The reported extended coordination polymers are based on a specific nitronyl nitroxide radical, NIT-4Py(2-(4-pyridyl)-4,4,5,5-tetramethylimidazoline-1-oxyl-3-oxide),[49-52] which behaves as a three-connecting linker for Ln(III) ions. This led to a unique two-dimensional networks with five-spin [$Ln_3(NIT)_2$] nodes, [{$Ln(tfa)_3$}$_3$(NIT-4Py)$_2$]$_n$ [Ln^{III} = Gd **1** and Tb **2**; tfa^- = trifluoroacetylacetonato]. The Tb derivative was found to exhibit SMM behavior in zero field, which was demonstrated by ac susceptibility data and the opening of an *M* versus *H* hysteresis loop.

EXPERIMENTAL SECTION

Materials and Characterizations. All reagents used in the reactions were obtained from commercial suppliers and directly employed without further purification. The radical ligand NIT-4Py was synthesized following established procedures.[49, 53] The FT-IR spectra were obtained using a The Bruker-Tenor 27 spectrometer. Elemental microanalyses for C, H, and N of solid complexes were conducted using a PerkinElmer 240 elemental analyzer. Powder X-ray diffraction (PXRD) patterns were obtained by a Rigaku SmartLab SE X-ray diffractometer(CuKα radiation). Magnetic measurements were carried out with MPMS XL-7 SQUID magnetometer and Physical Property Measurement System (PPMS, Quantum Design) using VSM or ACMS configuration for either DC or AC measurements. Magnetic susceptibility data were collected in a field of 1 kOe and 50 Oe, and isothermal magnetization were

recorded up to 70 kOe. The sample was mixed to grease and hold in a medical capsule for Tb derivative. The susceptibility data have been corrected for the diamagnetic contributions of the holder and all the atoms using the Pascal tables.[54]

Preparation of [{Ln(tfa)$_3$}$_3$(NIT-4Py)$_2$]$_n$ (Ln = Gd 1 and Tb 2)

Both complexes **1** and **2** were prepared using the same procedure: Ln(tfa)$_3$·3H$_2$O (0.45 mmol) was dissolved in 30 mL of n-heptane and heated under reflux for 3 hours. The solution was then cooled to 85°C and 5 mL of dichloromethane solution containing NIT-4Py (0.3 mmol) was added. The mixture was refluxed for another hour, allowed to cool to room temperature, filtered, and the filtrate was left at room temperature. After two days, deep blue crystals suitable for X-ray diffraction analysis were obtained.

[{Gd(tfa)$_3$}$_3$(NIT-4Py)$_2$]$_n$ (**1**): Yield: 70%. Anal. Calc. For $C_{138}O_{44}N_{12}H_{136}F_{54}Gd_6$: C, 35.75; H, 2.96; N, 3.63%. Found: C, 35.99; H, 3.25; N, 3.46%. IR: (KBr, cm^{-1}): 3447(w), 1632(s), 1527(m), 1491(w), 1401(w), 1370(m), 1292(s), 1223(m), 1188(s), 1137(s), 1009(w), 853(w), 779(w), 726(w), 560(w).

[{Tb(tfa)$_3$}$_3$(NIT-4Py)$_2$]$_n$ (**2**): Yield: 75%. Anal. Calc. For $C_{138}O_{44}N_{12}H_{136}F_{54}Tb_6$: C, 35.67; H, 2.95; N, 3.62%. Found: C, 35.71; H, 2.65; N, 3.65%. IR: (KBr, cm^{-1}): 3445(w), 1634(s), 1528(m), 1399(w), 1371(s), 1294(s), 1224(m), 1187(m), 1138(s), 854(m), 780(w), 727(m), 561(w).

The experimental PXRD patterns of **1** and **2** are consistent with the simulated patterns (Figure S1), which confirms the phase purity of crystalline samples.

X-ray crystallography

The crystallographic data for complexes **1** and **2** were acquired using Cu-Kα radiation on a Rigaku Saturn CCD diffractometer, and the Olex2 software package,[55] containing the SHELXT-2018[56] structure solution program and SHELXL-2018,[57] was employed for the analysis and refinement of all structures. Non-hydrogen atoms underwent refinement for anisotropic displacement parameters using a full-matrix

least-squares method, while the positions of hydrogen atoms were determined from refinement cycles with geometric restraints. To rationalize some unordered atoms, restraints of ISOR, DELU, or SIMU were used. It was discovered that both complexes are twins, and twin rotation matrix for batch 2 are -1 0 0 -0 -0.998 -0.5 0.002-0.008 0.998 (BASF:0.1268) for **1** and -1.000 0 0 -0 -1 0.5 -0.001-0.002 1 (BASF:0.5550) for **2**. The crystallographic refinement details for **1** and **2** can be found in Table 1, whereas the significant bond lengths and angles are provided in Tables S2 and S3.

Table 1. Crystallographic data and structure refinement summary for **1** and **2**.

complex	**1**	**2**
formula	$C_{138}H_{136}F_{54}Gd_6N_{12}O_{44}$	$C_{138}H_{136}F_{54}N_{12}O_{44}Tb_6$
T/K	113	100
Crystal system	triclinic	triclinic
Space group	$P\bar{1}$	$P\bar{1}$
a/Å	15.5703(2)	15.5373(2)
b/Å	22.1153(5)	22.0532(3)
c/Å	27.0149(4)	27.0631(3)
α/°	107.598(2)	72.087(1)
β/°	90.063(1)	89.971(1)
γ/°	101.713(2)	78.481(1)
V/Å^3	8662.9(3)	8627.4(2)
Z	2	2
ρ_{calc}/g·cm^3	1.777	1.788
μ/mm^{-1}	15.811	13.052
F(000)	4540	4552
2Θ range /°	3.438 to 130.178	3.438 to 149.112
Reflections collected	29298	33549
Unique reflns	29298	33549
Data/restraints/parameters	29298/2475/2289	33549/1444/2404
GOF (F^2)	1.099	1.078
R_1/wR_2	0.1153/0.2319	0.0843/0.2310
R_1/wR_2 (all data)[a]	0.1331/0.2412	0.0992/0.2426

[a] $R_1 = \Sigma(||Fo| - |Fc||)/\Sigma|Fo|$, $wR_2 = [\Sigma w(|Fo|^2 - |Fc|^2)^2/\Sigma w(|Fo|^2)^2]^{1/2}$

Table 2. Key bond parameters(bond lengths (Å) and angles (°)) for **1** and **2**

Complex	**1**	**2**
Ln–O_{rad}	2.431(12)–2.499(12)	2.414(7)–2.497(7)
Ln–O_{tfa}	2.316(12)–2.382(11)	2.314(7)–2.38(1)
Ln–N	2.620(7)–2.627(7)	2.574(9)–2.620(8)
Ln–O–N	131.05(7)–141.59(8)	131.72(1)–141.13(2)

RESULTS AND DISCUSSION

Synthesis. Seminal investigation on Ln-NIT-4Py radical complexes were reported in 1990s by Gatteschi et al,[58] and same group described in 2007 the Dy-NIT-4Py complex, which exhibits SMM behavior.[40] Our group also obtained a series of Ln-radical complexes using the same radical but with different Ln(III) ions or co-ligands.[59, 60] A common feature off all these Ln-NIT-4Py complexes is their cyclic dimer structure. In this work, tfa^- was involved as co-ligand of Ln(III) unit resulting in the coordination networks $[\{Ln(tfa)_3\}_3(NIT\text{-}4Py)_2]_n$ (Ln = Gd, **1**, and Tb, **2**). These were obtained as a unique product under reaction conditions (solvent, temperature and metal/radical ratio) similar to those used in previous reports. This underlines the effect that subtle modifications at the periphery of the coordination centers can have on supramolecular assembly.

Crystal Structures. The studies of the X-ray crystal structures reveal that complexes **1** and **2** crystallize in the space groups $P\bar{1}$ (Table 1), and both are 2D coordination networks. The key bond parameters of **1** and **2** are listed in Table 2. The asymmetric unit of two complexes encompasses six crystallographically independent Ln^{III} ions and four NIT-4Py linkers (Figure 1). Specifically, all Ln^{III} ions are eight-coordinated with six O-atoms from three chelating tfa^- anions and either two oxygens from the NIT moieties of two radicals (Ln2 and Ln5), or one O-atom from a NIT and one N-atom from a pyridyl group of two distinct NIT-4Py (Ln1, Ln3, Ln5, and Ln6). The

coordination polyhedrons (Figure S3) of the Ln centers have distorted triangular dodecahedral (D_{2d}) geometry (see Table S3 for shape analysis details). The Ln–O_{tfa} and Ln–O_{rad} bond lengths respectively fall within the range of 2.316(12) Å–2.382(11) Å and 2.431(12) Å–2.499(12) Å for **1**, 2.314(7) Å–2.38(1) Å and 2.414(7) Å–2.497(7) Å for **2**. The Ln–N bond distances are in the range of 2.620(7) Å–2.627(7) Å for **1** and 2.574(9) Å–2.620(8) Å for **2**, which is longer than those of Ln–O_{tfa} and Ln–O_{rad} bond lengths (table 2). Each NIT-4Py radical acts as a tri-dentate ligand linked to three Ln^{III} ions in μ_3-η^1:η^1:η^1-coordination mode, by means of both the NO groups and the pyridine N atom, resulting in a two-dimensional network. In these 2D network, two NIT-4Py linkers connect three Ln^{III} ions with nitronyl nitroxides (NIT), forming a linear [$Ln_3(NIT)_2$] node with [4f-NIT-4f-NIT-4f] array (Figure. 2). Each node is connected to four adjacent nodes by the means of pyridyl groups. The distances between two Ln^{III} ions through the NIT moiety in **1** and **2** are vary from 8.528 Å–8.835 Å and 8.508 Å–8.781 Å, respectively. The two-dimensional 2*p*-4*f* layers stack along the *b*-direction with the minimum Ln–Ln distances of 11.125 Å for **1** and 10.440 Å for **2** (Figure. S4).

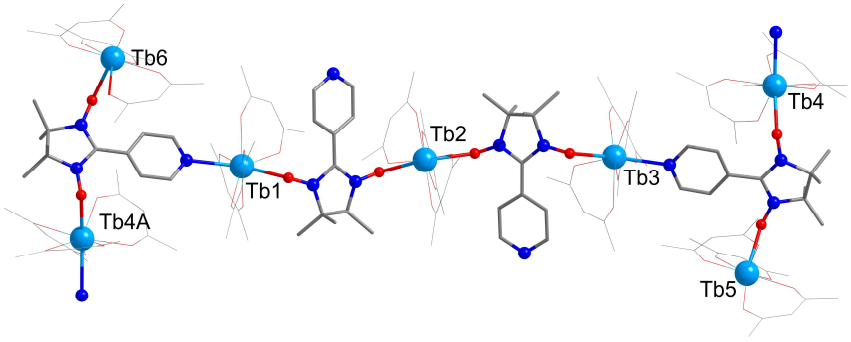

Figure 1. The asymmetric unit of **2** (H and F atoms are omitted for clarity).

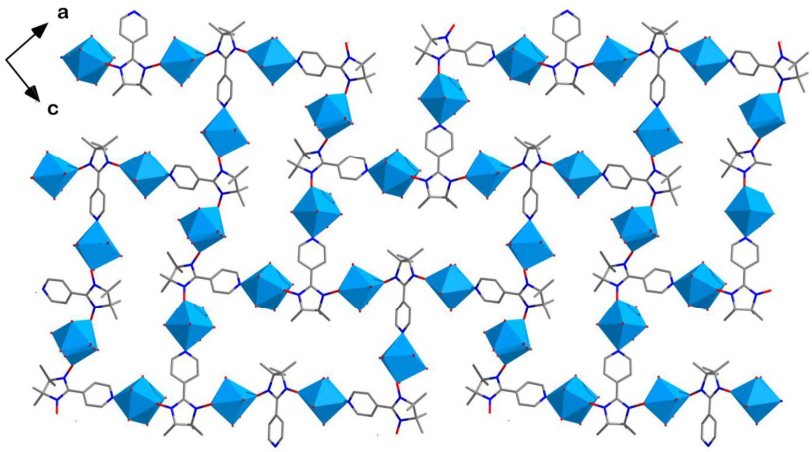

Figure 2. View of the $[\{Tb(tfa)_3\}_3(NIT\text{-}4Py)_2]_n$ network.

Magnetic Properties. From a magnetic view point, the present polymeric system comes down to the five spin species $[Ln_3(NIT)_2]$. Indeed, while an exchange interaction between NIT and the Ln centers linked by the aminoxyl groups might be expected (i.e. within the [4f-NIT-4f-NIT-4f] array), only very weak, if any, exchange interaction is anticipated to be mediated by the pyridyl groups. Therefore the magnetic data below are given with respect to a $[Ln_3(NIT)_2]$ unit.

The dc magnetic susceptibilities of complexes **1** and **2** were measured between 2-300 K in a field of 1 kOe (Figure 3 and 4). At 300 K, the $\chi_M T$ products (χ_M stands for the magnetic susceptibility of a Ln_3NIT_2 moiety) of 24.83 cm^3Kmol^{-1} for **1** and 36.30 cm^3Kmol^{-1} for **2**, are close to the theoretical values of 24.39 cm^3Kmol^{-1} and 36.15 cm^3Kmol^{-1}, respectively, for an uncoupled system comprising three Ln^{III} ions (Gd^{III}: $^8S_{7/2}$, S = 7/2, L = 0, C = 7.88 cm^3 K mol^{-1}; Tb^{III}: $^7F_6$, S = 3, L =3, C = 11.82 cm^3Kmol^{-1}) and two radical species (S = 1/2, C = 0.375 cm^3Kmol^{-1}). Upon decreasing the temperature, the $\chi_M T$ gradually increases to reach 71.90 cm^3Kmol^{-1} at 2 K for **1** and a maximum of 144.6 cm^3Kmol^{-1} at 3.0 K for **2** before dropping sharply to 128 cm^3Kmol^{-1} at 2 K. Such behaviors are characteristic for ferromagnetic interactions between the spin centers. For **2**, the down-turn of $\chi_M T$ at low T (black trace) is no longer found in a weaker field strength (50 Oe, blue trace), with $\chi_M T$ steadily increasing to 363.6 cm^3Kmol^{-1} at 2.0 K. Thus the maximum can be attributed

to an effect of saturation rather than to antiferromagnetic interactions. The field dependence of the magnetizations for both complexes show a rapid increase for low fields before leveling and reaching 22.65 Nβ (2.0 K; 70 kOe) for **1** (Figure 3 inset) and 16.4 Nβ (2.4 K; 70 kOe) for **2** (Figure S5). The magnetization at saturation for **1** is in good agreement with the 23 Nβ expected for S = 23/2, confirming ferromagnetic NIT-Gd interactions.

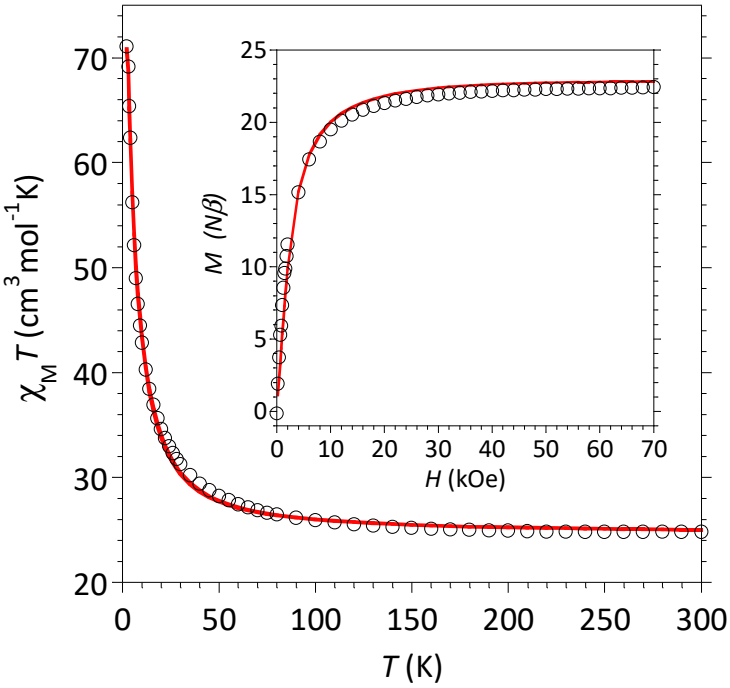

Figure 3. Plot of $\chi_M T$ versus T and (inset) M versus H curve for **1**. The red line is the simulation curve by PHI.

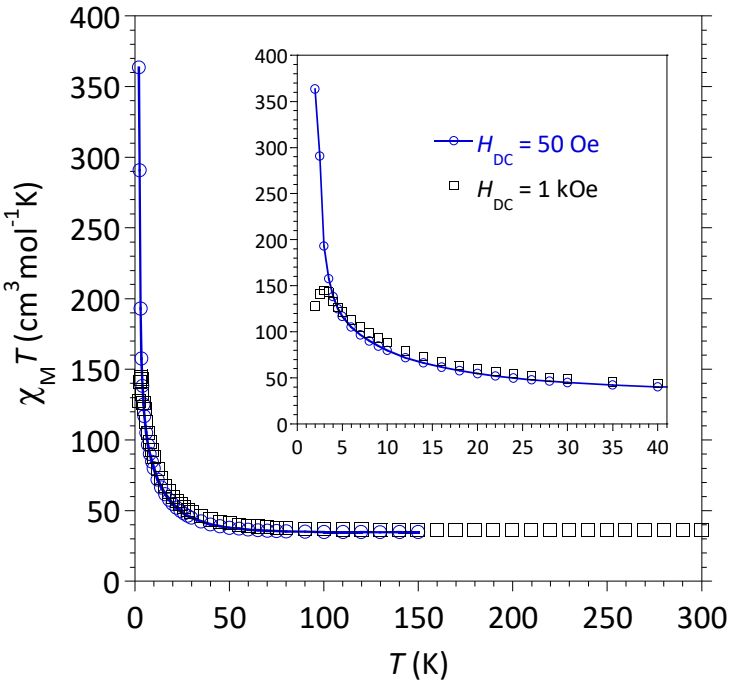

Figure 4. $\chi_M T$ *versus* T curves with H_{DC} = 1 kOe (black) and 50 Oe for **2**. The insert shows the low T range behaviors.

Accordingly, the magnetic data for **1** could be quantitatively analyzed by considering the exchange interaction outlined in scheme 1. There, J_1 is the magnetic coupling between a nitroxyl group and a Gd^{III} ion and J_2 represents exchange between two next-neighbor aminoxyl groups through the Gd^{III} ion. A possible contribution from magnetic exchange between the $[Gd_3NIT_2]$ units mediated the pyridine rings was considered within the mean-field approximation (zJ').[61] The PHI software[62] was used to simultaneously fit $\chi_M T$ versus T and M versus H curves based on the Hamiltonian:

$$\hat{H} = -2J_1\left(\hat{S}_{Gd1}\hat{S}_{Rad1} + \hat{S}_{Rad1}\hat{S}_{Gd2} + \hat{S}_{Gd2}\hat{S}_{Rad2} + \hat{S}_{Rad2}\hat{S}_{Gd3}\right) - 2J_2\left(\hat{S}_{Rad1}\hat{S}_{Rad2}\right) + \beta H g_{rad}\left(\hat{S}_{Gd1} + \hat{S}_{Gd2} + \hat{S}_{Gd3}\right) + \beta H g_{rad}\left(\hat{S}_{Rad1} + \hat{S}_{Rad2}\right)$$

, yielding J_1 = 3.74(4) cm^{-1}, J_2 = -8.8(2) cm^{-1}, g_{Gd} = 1.99(1), g_{rad} = 2.0 (fixed) and zJ' = 0.00295(2) cm^{-1}.

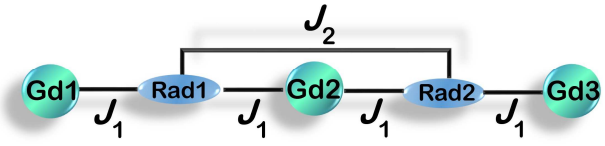

Scheme 1. Magnetic exchange pathway of **1**.

The positive J_1 indicates ferromagnetic interactions between the Gd^{III} ion and the

coordinated NO group, its value is comparable to the exchange interactions reported in the literature.[58, 63] The negative J_2 is in line with antiferromagnetic exchange between the coordinated NO groups via Gd reported before; its strength is in agreement with reported values.[63, 64] Finally, the insignificant zJ' parameter confirms the absence of magnetic interactions between the $[Gd_3NIT_2]$ units.

AC-susceptibility studies showed no out-of-phase susceptibility (χ_M'') signal for **1**, thus excluding magnetic ordering in the investigated temperature domain (Figure S6). For **2**, temperature / frequency dependence peaks of in-phase (χ_M') and out-of-phase (χ_M'') susceptibility components were observed in the temperature range of 2.0 to 14.0 K without an applied static field (Figure 5 and S7), indicating SMM behavior. Application of a static DC did not change the observed behaviors (Figure. S8). The Cole–Cole plot (Figure 6a) show a near symmetrical shape; its analysis by the generalized Debye model[65] gave α parameters of 0.062–0.081, indicating a very narrow distribution of relaxation times.

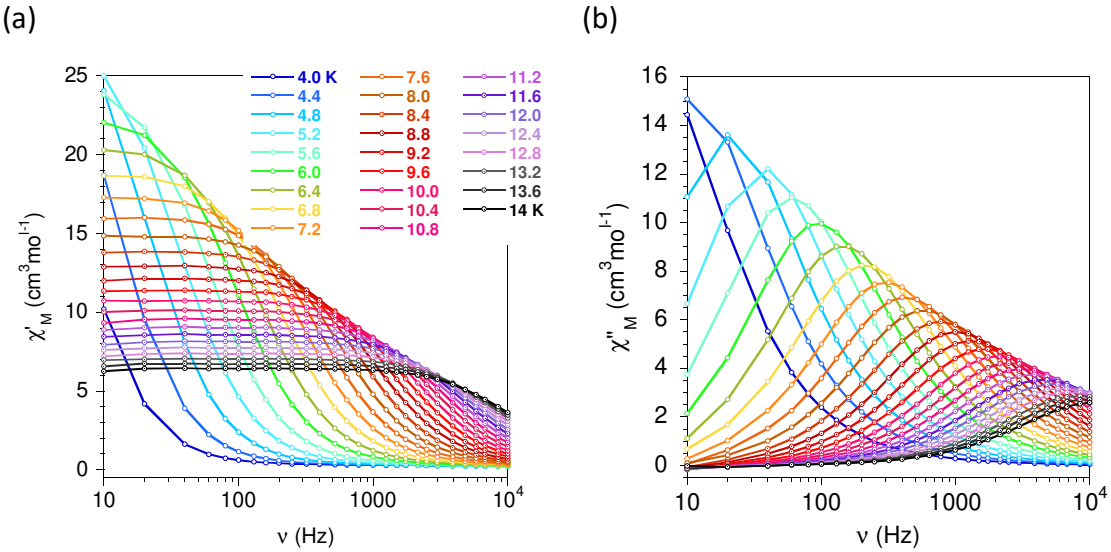

Figure 5. Frequency dependence (from 10–10^4 Hz) of the (a) in-phase and (b) out-of-phase ac susceptibility in the absence of an applied dc field for **2**.

The temperature dependence of the relaxation time (τ) extracted from the frequency-

dependent ac susceptibility data with the generalized Debye model is shown in Figure. 6b. The relaxation behavior is well reproduced by considering Raman and Orbach relaxation processes, respectively first and second term in $\tau^{-1} = CT^{n} + \tau_0^{-1} \exp(-U_{eff}/k_BT)$. Best fit led to an effective energy barrier U_{eff} = 53.8(6) K, τ_0 = 6.8(9) × 10^{-7}s, C = 0.025(5)6 $s^{-1}K^{-n}$ and n = 5.4. The energy barrier for spin reversal for **2** is among the largest found in discrete Tb-NIT derivatives (Table S4).[28, 59, 66, 67] The exponent n is lower than the value expected for non-Kramers systems (n = 7) but this is commonly found in Ln^{III} SMMs, [68-72] and is attributed to optical and acoustic phonons.[73, 74] Theoretical investigation by Gu *et al*. suggests that a combination of several low-energy molecular vibrations can contribute to the lower exponent of the temperature dependence in the Raman relaxation mechanism.[75, 76]

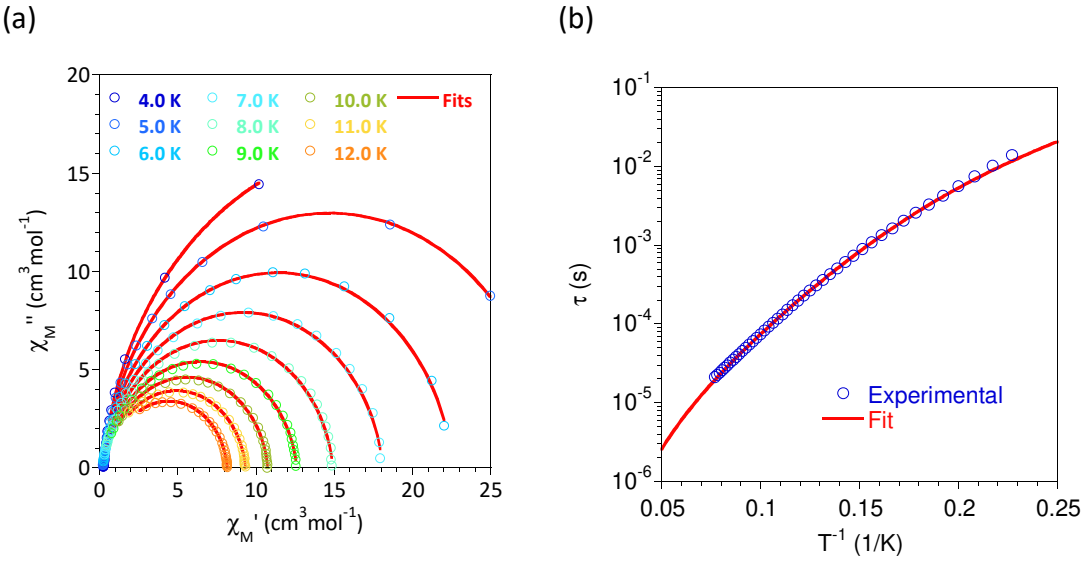

Figure 6. (a) Cole–Cole diagrams at different temperatures under zero dc field for **2**; (b) Fitting of the Arrhenius plot based on equation $\ln\tau = -\ln[CT^{n} + \tau_0^{-1}\exp(-U_{eff}/k_BT)]$.

The ZFC-FC magnetizations for **2** exhibit a clear divergence below 2.4 K (Figure 7a), suggesting a blocking of the magnetization (T_B = 2.4 K). This is supported by the opening of a hysteresis loop with a coercive field 110 Oe at 2.3 K (Figure 7b), a hallmark of SMM. To date, few Ln-Nitroxide SMMs exhibit hysteresis loop[29, 42, 67, 77]

and most of their hysteresis loops are observed at extremely low temperatures (< 2 K). Recent studies have shown that the Raman relaxation, responsible for relaxation under the barrier, is directly linked to ligand vibrations.[78] In order to support a possible role of the stiffness of the lattice on the magnetic relaxation behavior of **2**, it is instructive to compare its SMM characteristics with the previously reported discrete Tb-NIT-4Py complexes, i.e. $[Tb(hfac)_3(NIT\text{-}4Py)]_2$[59] and $[Tb(Phtfac)_3(NIT\text{-}4Py)]_2$.[60] For the first, no slow relaxation of the magnetization was observed above 2 K, whereas second exhibited an Orbach type relaxation with a barrier of 25.7(4) K, to be compared with the 53.8 K obtained for complex **2**. Thus, the better SMM behavior of **2** can be attributed to a clear reduction of the under the barrier relaxation. This result suggests that embedding the spin cluster (i.e. $[Tb_3(NIT)_2]$) in an extended, stiffer lattice limits the contributions of molecular vibrations to the relaxation of the magnetization.

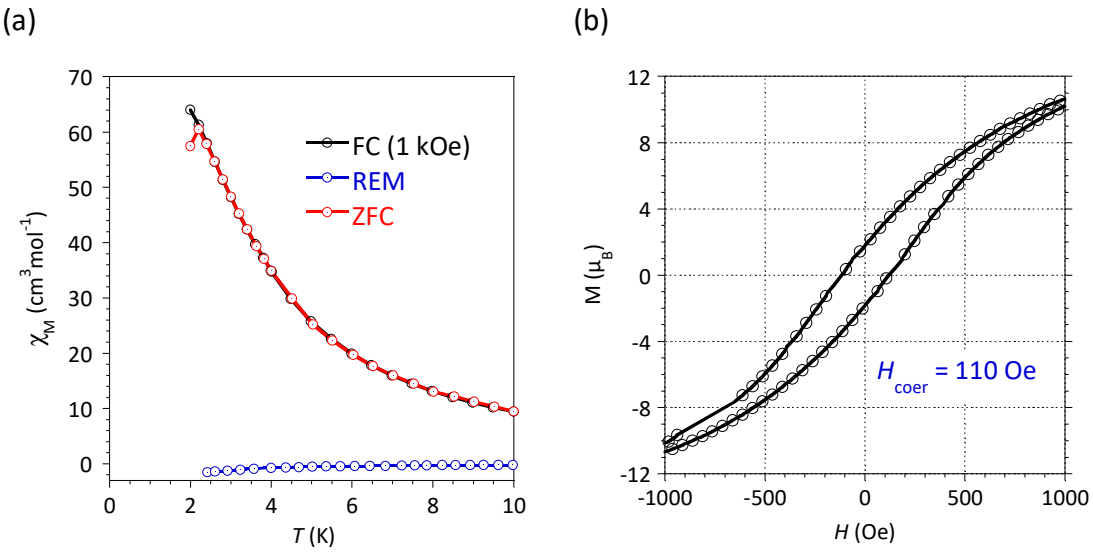

Figure 7. Plots of (a) the field cooled (FC), zero field cooled (ZFC), and remnant magnetization (REM) recorded with an applied field of 1 kOe for **2**; (b) hysteresis loops of polycrystalline sample at T = 2.3 K for **2**. The field scan rate was constant at 33 Oe/s.

CONCLUSION

The use of NIT-4Py radical behaving as a 3-connection linker to coordinate to the Ln^{III} ions, allowed the formation of an unique two-dimensional network made up by five-spin $[Ln_3(NIT)_2]$ nodes. Importantly, ferromagnetic Ln-NIT interactions take place between the five centers but the nodes are magnetically well isolated. The Tb derivative was found to behave as a field-free SMM with an energy barrier for spin flipping among the largest known the Tb-NIT SMMs. For this complex, a blocking temperature of about 2.3 K gave rise to the opening of a hysteresis loop. To the best of our knowledge, this is the first example of an SMM network based on Ln-nitronyl nitroxide. These results open up interesting prospects for the design of a new generation of molecular nanomagnets based on the Ln-Radical combination.

ASSOCIATED CONTENT

Supporting Information

Synthetic details, structural data, PXRD, and additional structural and magnetic figures.

Crystallographic data for **1** and **2** (CIF).

Accession Codes

CCDC 2351608 and 2351609 include the complementary crystallographic data in this paper. These data could be obtained free of charge via www.ccdc.cam.ac.uk/data_request/cif, or by emailing data_request@ccdc.cam.ac.uk, or by contacting The Cambridge Crystallographic Data Centre, 12 Union Road, Cambridge CB2 1EZ, UK; fax: + 44 1223 336033.Relevant data can be obtained by www.ccdc.cam.ac.uk/data_request/cif.

AUTHOR INFORMATION

Corresponding Authors

Licun Li – *Department of Chemistry, Key Laboratory of Advanced Energy Materials Chemistry, College of Chemistry, Nankai University, Tianjin 300071, China*; orcid: 0000-0001-8380-2946; E-mail: llicun@nankai.edu.cn

Xue-Lan Mei – *College of Materials Science and Chemical Engineering, Bengbu University, Bengbu, 233030, P. R. China*; E-mail: 412242927@qq.com

Jean-Pascal Sutter – *Laboratoire de Chimie de Coordination du CNRS (LCC-CNRS), Université de Toulouse, CNRS, Toulouse, France;* orcid: 0000-0003-4960-0579; E-mail: jean-pascal.sutter@lcc-toulouse.fr

Authors

Chao-Yi Jin – *Department of Chemistry, Key Laboratory of Advanced Energy Materials Chemistry, College of Chemistry, Nankai University, Tianjin 300071, China*

Yan Zhou – *Department of Chemistry, Key Laboratory of Advanced Energy Materials Chemistry, College of Chemistry, Nankai University, Tianjin 300071, China*

Notes

There are no conflicts to declare.

ACKNOWLEDGMENTS

Financial supports from the National Natural Science Foundation of China (No. 21773122). Authors are grateful to Dr. L.-M. Lacroix and to Mrs G. Ballon (INSA Toulouse) for technical assistance in magnetic data collections.

REFERENCES

(1) Rinehart, J. D.;Long, J. R. Exploiting single-ion anisotropy in the design of f-element single-molecule magnets. *Chem. Sci* **2011**, *2* (11), 2078-2085.

(2) Woodruff, D. N.; Winpenny, R. E. P.;Layfield, R. A. Lanthanide Single-Molecule Magnets. *Chem. Rev.* **2013**, *113* (7), 5110-5148.

(3) Ungur, L.; Le Roy, J. J.; Korobkov, I.; Murugesu, M.;Chibotaru, L. F. Fine-tuning the Local Symmetry to Attain Record Blocking Temperature and Magnetic Remanence in a Single-Ion Magnet. *Angew. Chem. Int. Ed.* **2014**, *53* (17), 4413-4417.

(4) Liu, J.-L.; Chen, Y.-C.;Tong, M.-L. Symmetry strategies for high performance lanthanide-based single-molecule magnets. *Chem. Soc. Rev.* **2018**, *47* (7), 2431-2453.

(5) Zhu, Z.; Zhao, C.; Feng, T.; Liu, X.; Ying, X.; Li, X.-L.; Zhang, Y.-Q.;Tang, J. Air-Stable Chiral Single-Molecule Magnets with Record Anisotropy Barrier Exceeding 1800 K. *J. Am. Chem. Soc.* **2021**, *143* (27), 10077-10082.

(6) Sutter, J.-P.; Béreau, V.; Jubault, V.; Bretosh, K.; Pichon, C.;Duhayon, C. Magnetic anisotropy of transition metal and lanthanide ions in pentagonal bipyramidal geometry. *Chem. Soc. Rev.* **2022**, *51* (8), 3280-3313.

(7) Zhu, Z.;Tang, J. Lanthanide single-molecule magnets with high anisotropy barrier: where to from here? *Natl. Sci. Rev.* **2022**, *9* (12), nwac194.

(8) Chen, Y.-C.; Liu, J.-L.; Ungur, L.; Liu, J.; Li, Q.-W.; Wang, L.-F.; Ni, Z.-P.; Chibotaru, L. F.; Chen, X.-M.;Tong, M.-L. Symmetry-Supported Magnetic Blocking at 20 K in Pentagonal Bipyramidal Dy(III) Single-Ion Magnets. *J. Am. Chem. Soc.* **2016**, *138* (8), 2829-2837.

(9) Guo, F.-S.; Day, B. M.; Chen, Y.-C.; Tong, M.-L.; Mansikkamäki, A.;Layfield, R. A. A Dysprosium Metallocene Single-Molecule Magnet Functioning at the Axial Limit. *Angew. Chem. Int. Ed.* **2017**, *56* (38), 11445-11449.

(10) Guo, F.-S.; Day, B. M.; Chen, Y.-C.; Tong, M.-L.; Mansikkamäki, A.;Layfield, R.

A. Magnetic hysteresis up to 80 kelvin in a dysprosium metallocene single-molecule magnet. *Science* **2018**, *362* (6421), 1400-1403.

(11) Gould, C. A.; McClain, K. R.; Reta, D.; Kragskow, J. G. C.; Marchiori, D. A.; Lachman, E.; Choi, E.-S.; Analytis, J. G.; Britt, R. D.; Chilton, N. F.; Harvey, B. G.;Long, J. R. Ultrahard magnetism from mixed-valence dilanthanide complexes with metal-metal bonding. *Science* **2022**, *375* (6577), 198-202.

(12) Hu, Z.; Wang, Y.; Ullah, A.; Gutiérrez-Finol, G. M.; Bedoya-Pinto, A.; Gargiani, P.; Shi, D.; Yang, S.; Shi, Z.; Gaita-Ariño, A.;Coronado, E. High-temperature magnetic blocking in a monometallic dysprosium azafullerene single-molecule magnet. *Chem* **2023**, *9* (12), 3613-3622.

(13) Zhu, Z.-H.; Paul, S.; Zhao, C.; Wu, J.-F.; Ying, X.; Ungur, L.; Wernsdorfer, W.; Meyer, F.;Tang, J.-K. Record Quantum Tunneling Time in an Air-Stable Exchange-Bias Dysprosium Macrocycle. *J. Am. Chem. Soc.* **2024**, *146* (28), 18899-18904.

(14) Liddle, S. T.;van Slageren, J. Improving f-element single molecule magnets. *Chem. Soc. Rev.* **2015**, *44* (19), 6655-6669.

(15) Lunghi, A.; Totti, F.; Sessoli, R.;Sanvito, S. The role of anharmonic phonons in under-barrier spin relaxation of single molecule magnets. *Nat. Commun.* **2017**, *8* (1), 14620.

(16) Yu, K.-X.; Kragskow, J. G. C.; Ding, Y.-S.; Zhai, Y.-Q.; Reta, D.; Chilton, N. F.;Zheng, Y.-Z. Enhancing Magnetic Hysteresis in Single-Molecule Magnets by Ligand Functionalization. *Chem* **2020**, *6* (7), 1777-1793.

(17) Mínguez Espallargas, G.;Coronado, E. Magnetic functionalities in MOFs: from the framework to the pore. *Chem. Soc. Rev.* **2018**, *47* (2), 533-557.

(18) Huang, G.; Fernandez-Garcia, G.; Badiane, I.; Camarra, M.; Freslon, S.; Guillou, O.; Daiguebonne, C.; Totti, F.; Cador, O.; Guizouarn, T.; Le Guennic, B.;Bernot, K. Magnetic Slow Relaxation in a Metal–Organic Framework Made of Chains of Ferromagnetically Coupled Single-Molecule Magnets. *Chem. Eur. J.* **2018**, *24* (27), 6983-6991.

(19) Wan, Q.; Wakizaka, M.;Yamashita, M. Single-ion magnetism behaviors in lanthanide(III) based coordination frameworks. *Inorg. Chem. Front.* **2023**, *10* (18), 5212-5224.

(20) Manna, F.; Oggianu, M.; Avarvari, N.;Mercuri, M. L. Lanthanide-Based Metal–Organic Frameworks with Single-Molecule Magnet Properties. *Magnetochemistry* **2023**, *9* (7), 190.

(21)Jeon, I.-R.;Clérac, R. Controlled association of single-molecule magnets (SMMs) into coordination networks: towards a new generation of magnetic materials. *Dalton Trans.* **2012**, *41* (32), 9569-9586.

(22) Zhang, X.; Vieru, V.; Feng, X.; Liu, J.-L.; Zhang, Z.; Na, B.; Shi, W.; Wang, B.-W.; Powell, A. K.; Chibotaru, L. F.; Gao, S.; Cheng, P.;Long, J. R. Influence of Guest Exchange on the Magnetization Dynamics of Dilanthanide Single-Molecule-Magnet Nodes within a Metal–Organic Framework. *Angew. Chem. Int. Ed.* **2015**, *54* (34), 9861-9865.

(23) Liu, K.; Zhang, X.; Meng, X.; Shi, W.; Cheng, P.;Powell, A. K. Constraining the coordination geometries of lanthanide centers and magnetic building blocks in frameworks: a new strategy for molecular nanomagnets. *Chem. Soc. Rev.* **2016**, *45* (9), 2423-2439.

(24) Sun, A.-H.; Liu, X.-X.; Sun, R.; Xiong, J.; Sun, H.-L.;Gao, S. The rational construction of diamond-like dysprosium–hexacyanometallate frameworks featuring dynamic magnetic behaviour. *Inorg. Chem. Front.* **2022**, *9*, 231-240.

(25) Kumar, K.; Li, G.; Stefanczyk, O.; Chorazy, S.; Nakabayashi, K.;Ohkoshi, S.-i. Slow magnetic relaxation in Nd(III) and Sm(III) complexes formed in three-dimensional lanthanide-dicyanidometallate(I) frameworks exhibiting luminescent properties. *J. Mater. Chem. C* **2023**, *11* (3), 1008-1020.

(26) Sessoli, R.;Bernot, K., Lanthanides in Extended Molecular Networks, *Lanthanides and Actinides in Molecular Magnetism*, 2015, pp. 89-124.

(27) Rinehart, J. D.; Fang, M.; Evans, W. J.;Long, J. R. A N_2^{3-} radical-bridged terbium complex exhibiting magnetic hysteresis at 14 K. *J. Am. Chem. Soc.* **2011**, *133*

(36), 14236-14239.

(28) Demir, S.; Jeon, I.-R.; Long, J. R.;Harris, T. D. Radical ligand-containing single-molecule magnets. *Coord. Chem. Rev.* **2015**, *289-290*, 149-176.

(29) Kanetomo, T.; Yoshii, S.; Nojiri, H.;Ishida, T. Single-molecule magnet involving strong exchange coupling in terbium(III) complex with 2,2′-bipyridin-6-yl tert-butyl nitroxide. *Inorg. Chem. Front.* **2015**, *2* (9), 860-866.

(30) Huang, G.; Daiguebonne, C.; Calvez, G.; Suffren, Y.; Guillou, O.; Guizouarn, T.; Le Guennic, B.; Cador, O.;Bernot, K. Strong Magnetic Coupling and Single-Molecule-Magnet Behavior in Lanthanide-TEMPO Radical Chains. *Inorg. Chem.* **2018**, *57* (17), 11044-11057.

(31) Mavragani, N.; Errulat, D.; Gálico, D. A.; Kitos, A. A.; Mansikkamäki, A.;Murugesu, M. Radical-Bridged Ln_4 Metallocene Complexes with Strong Magnetic Coupling and a Large Coercive Field. *Angew. Chem. Int. Ed.* **2021**, *60* (45), 24206-24213.

(32) Inoue, K.; Hayamizu, T.; Iwamura, H.; Hashizume, D.;Ohashi, Y. Assemblage and Alignment of the Spins of the Organic Trinitroxide Radical with a Quartet Ground State by Means of Complexation with Magnetic Metal Ions. A Molecule-Based Magnet with Three-Dimensional Structure and High T_C of 46 K. *J. Am. Chem. Soc.* **1996**, *118* (7), 1803-1804.

(33) Fegy, K.; Luneau, D.; Ohm, T.; Paulsen, C.;Rey, P. Two-Dimensional Nitroxide-Based Molecular Magnetic Materials. *Angew. Chem. Int. Ed.* **1998**, *37* (9), 1270-1273.

(34) Motokawa, N.; Miyasaka, H.; Yamashita, M.;Dunbar, K. R. An Electron-Transfer Ferromagnet with T_c=107 K Based on a Three-Dimensional $[Ru2]_2$/TCNQ System. *Angew. Chem. Int. Ed.* **2008**, *47* (40), 7760-7763.

(35) Miller, J. S. Magnetically ordered molecule-based materials. *Chem. Soc. Rev.* **2011**, *40* (6), 3266-3296.

(36) Luneau, D. Coordination Chemistry of Nitronyl Nitroxide Radicals Has Memory. *Eur. J. Inorg. Chem.* **2020**, *2020* (7), 597-604.

(37) Perlepe, P.; Oyarzabal, I.; Mailman, A.; Yquel, M.; Platunov, M.; Dovgaliuk, I.; Rouzières, M.; Négrier, P.; Mondieig, D.; Suturina, E. A.; Dourges, M.-A.; Bonhommeau, S.; Musgrave, R. A.; Pedersen, K. S.; Chernyshov, D.; Wilhelm, F.; Rogalev, A.; Mathonière, C.;Clérac, R. Metal-organic magnets with large coercivity and ordering temperatures up to 242°C. *Science* **2020**, *370* (6516), 587-592.

(38) Thorarinsdottir, A. E.;Harris, T. D. Metal–Organic Framework Magnets. *Chem. Rev.* **2020**, *120* (16), 8716-8789.

(39) Bernot, K.; Bogani, L.; Caneschi, A.; Gatteschi, D.;Sessoli, R. A Family of Rare-Earth-Based Single Chain Magnets: Playing with Anisotropy. *J. Am. Chem. Soc.* **2006**, *128* (24), 7947-7956.

(40) Poneti, G.; Bernot, K.; Bogani, L.; Caneschi, A.; Sessoli, R.; Wernsdorfer, W.;Gatteschi, D. A rational approach to the modulation of the dynamics of the magnetisation in a dysprosium–nitronyl-nitroxide radical complex. *Chem. Commun.* **2007**, *18* (18), 1807-1809.

(41) Bernot, K.; Pointillart, F.; Rosa, P.; Etienne, M.; Sessoli, R.;Gatteschi, D. Single molecule magnet behaviour in robust dysprosium–biradical complexes. *Chem. Commun.* **2010**, *46* (35), 6458-6460.

(42) Coronado, E.; Giménez-Saiz, C.; Recuenco, A.; Tarazón, A.; Romero, F. M.; Camón, A.;Luis, F. Single-Molecule Magnetic Behavior in a Neutral Terbium(III) Complex of a Picolinate-Based Nitronyl Nitroxide Free Radical. *Inorg. Chem.* **2011**, *50* (16), 7370-7372.

(43) Pointillart, F.; Bernot, K.; Poneti, G.;Sessoli, R. Crystal Packing Effects on the Magnetic Slow Relaxation of Tb(III)-Nitronyl Nitroxide Radical Cyclic Dinuclear Clusters. *Inorg. Chem.* **2012**, *51* (22), 12218-12229.

(44) Hu, P.; Wang, X.; Ma, Y.; Wang, Q.; Li, L.;Liao, D. A new family of Ln–radical chains (Ln = Nd, Sm, Gd, Tb and Dy): synthesis, structure, and magnetic properties. *Dalton Trans.* **2014**, *43* (5), 2234-2243.

(45) Xiao, Z.-X.; Miao, H.; Shao, D.; Wei, H.-Y.; Zhang, Y.-Q.;Wang, X.-Y. Single-

molecule magnet behaviour in a dysprosium-triradical complex. *Chem. Commun.* **2018**, *54* (70), 9726-9729.

(46) Liu, X.; Zhang, Y.; Shi, W.;Cheng, P. Rational Design and Synthesis of a Chiral Lanthanide-Radical Single-Chain Magnet. *Inorg. Chem.* **2018**, *57* (21), 13409-13414.

(47) Shi, J.-Y.; Wu, M.-Z.; Chen, P.-Y.; Li, T.; Tian, L.;Zhang, Y.-Q. Terbium Triangle Bridged by a Triazole Nitronyl Nitroxide Radical with Single-Molecule-Magnet Behavior. *Inorg. Chem.* **2019**, *58* (21), 14285-14288.

(48) Li, H.-D.; Wu, S.-G.;Tong, M.-L. Lanthanide–radical single-molecule magnets: current status and future challenges. *Chem. Commun.* **2023**, *59* (41), 6159-6170.

(49) Caneschi, A.; Ferraro, F.; Gatteschi, D.; Rey, P.;Sessoli, R. Crystal structure and magnetic properties of a copper(II) chloride nitronyl nitroxide complex containing six exchange-coupled S = 1/2 spins. *Inorg. Chem.* **1990**, *29* (9), 1756-1760.

(50) Caneschi, A.; Gatteschi, D.; Sessoli, R.;Rey, P. Structure and magnetic properties of a ring of four spins formed by manganese(II) and a pyridine substituted nitronyl nitroxide. *Inorg. Chim. Acta* **1991**, *184* (1), 67-71.

(51) Caneschi, A.; Ferraro, F.; Gatteschi, D.; Rey, P.;Sessoli, R. Structure and magnetic properties of a chain compound formed by copper(II) and a tridentate nitronyl nitroxide radical. *Inorg. Chem.* **1991**, *30* (16), 3162-3166.

(52) Caneschi, A.; Gatteschi, D.; Rey, P.;Sessoli, R. Ordered bimetallic-radical species forming low-dimensional magnetic materials. *Chem. Mater.* **1992**, *4* (1), 204-209.

(53) Davis, M. S.; Morokuma, K.;Kreilick, R. W. Free radicals with large negative spin densities. *J. Am. Chem. Soc.* **1972**, *94* (16), 5588-5592.

(54) Kahn, O. *Molecular Magnetism*; VCH: Weinheim, Germany, 1993.

(55) Dolomanov, O. V.; Bourhis, L. J.; Gildea, R. J.; Howard, J. A. K.;Puschmann, H. OLEX2: a complete structure solution, refinement and analysis program. *J. Appl. Crystallogr.* **2009**, *42* (2), 339-341.

(56) Sheldrick, G. SHELXT - Integrated space-group and crystal-structure determination. *Acta Crystallogr. Sect. A: Found. Adv.* **2015**, *71* (1), 3-8.

(57) Sheldrick, G. Crystal structure refinement with SHELXL. *Acta Crystallogr. Sect. C: Struct. Chem.* **2015**, *71* (1), 3-8.

(58) Benelli, C.; Caneschi, A.; Gatteschi, D.;Pardi, L. Gadolinium(III) complexes with pyridine-substituted nitronyl nitroxide radicals. *Inorg. Chem.* **1992**, *31* (5), 741-746.

(59) Tian, H.-X.; Liu, R.-N.; Wang, X.-L.; Yang, P.-P.; Li, Z.-X.; Li, L.-C.;Liao, D.-Z. Magnetic Slow Relaxation in Cyclic Tb^{III}-Nitronyl Nitroxide Radical Complexes. *Eur. J. Inorg. Chem.* **2009**, *2009* (29-30), 4498-4502.

(60) Mei, X.-L.; Liu, R.-N.; Wang, C.; Yang, P.-P.; Li, L.-C.;Liao, D.-Z. Modulating spin dynamics of cyclic Ln^{III}-radical complexes (Ln^{III} = Tb, Dy) by using phenyltrifluoroacetylacetonate coligand. *Dalton Trans.* **2012**, *41* (10), 2904-2909.

(61) O'Connor, C. J., Magnetochemistry—Advances in Theory and Experimentation, *Prog. Inorg. Chem.*, 1982, vol. 29, pp. 203-283.

(62) Chilton, N. F.; Anderson, R. P.; Turner, L. D.; Soncini, A.;Murray, K. S. PHI: A powerful new program for the analysis of anisotropic monomeric and exchange-coupled polynuclear d- and f-block complexes. *J. Comput. Chem.* **2013**, *34* (13), 1164-1175.

(63) Sutter, J.-P.; Kahn, M. L.; Golhen, S.; Ouahab, L.;Kahn, O. Synthesis and Magnetic Behavior of Rare-Earth Complexes with N,O-Chelating Nitronyl Nitroxide Triazole Ligands: Example of a $[Gd^{III}\{Organic\ Radical\}_2]$ Compound with an S=9/2 Ground State. *Chem. Eur. J.* **1998**, *4* (4), 571-576.

(64) Xia, C.-C.; Ji, W.-J.; Zhang, X.-Y.; Miao, H.; Zhang, Y.-Q.;Wang, X.-Y. Syntheses, structures, and magnetic properties of the lanthanide complexes of imidazole-substituted nitronyl nitroxide biradicals. *Dalton Trans.* **2022**, *51* (32), 12362-12372.

(65) Aubin, S. M. J.; Sun, Z.-M.; Pardi, L.; Krzystek, J.; Folting, K.; Brunel, L.-C.; Rheingold, A. L.; Christou, G.;Hendrickson, D. N. Reduced Anionic Mn_{12}

Molecules with Half-Integer Ground States as Single-Molecule Magnets. *Inorg. Chem.* **1999**, *38* (23), 5329-5340.

(66) Wang, X.-L.; Li, L.-C.;Liao, D.-Z. Slow Magnetic Relaxation in Lanthanide Complexes with Chelating Nitronyl Nitroxide Radical. *Inorg. Chem.* **2010**, *49* (11), 4735-4737.

(67) Houard, F.; Gendron, F.; Suffren, Y.; Guizouarn, T.; Dorcet, V.; Calvez, G.; Daiguebonne, C.; Guillou, O.; Le Guennic, B.; Mannini, M.;Bernot, K. Single-chain magnet behavior in a finite linear hexanuclear molecule. *Chem. Sci* **2021**, *12* (31), 10613-10621.

(68) Wang, J.; Ruan, Z.-Y.; Li, Q.-W.; Chen, Y.-C.; Huang, G.-Z.; Liu, J.-L.; Reta, D.; Chilton, N. F.; Wang, Z.-X.;Tong, M.-L. Slow magnetic relaxation in a $\{EuCu_5\}$ metallacrown. *Dalton Trans.* **2019**, *48* (5), 1686-1692.

(69) Handzlik, G.; Magott, M.; Arczyński, M.; Sheveleva, A. M.; Tuna, F.; Baran, S.;Pinkowicz, D. Identical anomalous Raman relaxation exponent in a family of single ion magnets: towards reliable Raman relaxation determination? *Dalton Trans.* **2020**, *49* (34), 11942-11949.

(70) Kapurwan, S.; Mondal, A.; Sahu, P. K.;Konar, S. Windmill-like Ln_4 Clusters [Ln = Tb(III) and Dy(III)] Bridged by $[\alpha\text{-}AsW_9O_{33}]^{9-}$ Unit Showing Zero-Field SMM Behavior: Experimental and Theoretical Investigation. *Inorg. Chem.* **2022**, *61* (44), 17459-17468.

(71) Jin, P.-B.; Luo, Q.-C.; Gransbury, G. K.; Vitorica-Yrezabal, I. J.; Hajdu, T.; Strashnov, I.; McInnes, E. J. L.; Winpenny, R. E. P.; Chilton, N. F.; Mills, D. P.;Zheng, Y.-Z. Thermally Stable Terbium(II) and Dysprosium(II) Bis-amidinate Complexes. *J. Am. Chem. Soc.* **2023**, *145* (51), 27993-28009.

(72) Selikhov, A. N.; Félix, G.; Lyubov, D. M.; Nelyubina, Y. V.; Cherkasov, A. V.; Sene, S.; Taydakov, I. V.; Metlin, M. T.; Tyutyunov, A. A.; Guari, Y.; Larionova, J.;Trifonov, A. A. Luminescent Er^{3+} based single molecule magnets with fluorinated alkoxide or aryloxide ligands. *Dalton Trans.* **2024**, *53* (14), 6352-6366.

(73) Singh, A.;Shrivastava, K. N. Optical-acoustic two-phonon relaxation in spin systems. *phys. stat. sol. (b)* **1979**, *95* (1), 273-277.

(74) Shrivastava, K. N. Theory of Spin–Lattice Relaxation. *phys. stat. sol. (b)* **1983**, *117* (2), 437-458.

(75) Gu, L.;Wu, R. Origins of Slow Magnetic Relaxation in Single-Molecule Magnets. *Phys. Rev. Lett.* **2020**, *125* (11), 117203.

(76) Gu, L.;Wu, R.-Q. Origin of the anomalously low Raman exponents in single molecule magnets. *Phys. Rev. B* **2021**, *103* (1), 014401.

(77) Murakami, R.; Ishida, T.; Yoshii, S.;Nojiri, H. Single-molecule magnet [Tb(hfac)$_3$(2pyNO)] (2pyNO = t-butyl 2-pyridyl nitroxide) with a relatively high barrier of magnetization reversal. *Dalton Trans.* **2013**, *42* (38), 13968-13973.

(78) Zhai, Y.-Q.;Zheng, Y.-Z. Vibronic barrier effect of magnetic relaxation in single-molecule magnets. *J. Mater. Chem. C* **2021**, *9* (26), 8096-8098.

Supplementary Information

Contents

Table S1. Selected bond distances (Å) for compound **1**.

1Gd			
Gd(6)-O(41)	2.324(15)	Gd(4)-O(20)	2.354(11)
Gd(6)-O(37)	2.332(15)	Gd(4)-O(19)	2.359(12)
Gd(6)-O(32)	2.351(12)	Gd(4)-O(10)	2.350(12)
Gd(6)-O(30)#3	2.454(11)	Gd(4)-N(1)#2	2.61(7)
Gd(6)-O(21)	2.415(11)	Gd(5)-O(9)	2.378(11)
Gd(6)-O(14)	2.344(12)	Gd(5)-O(7)	2.335(11)
Gd(6)-O(1)	2.365(12)	Gd(5)-O(43)	2.499(11)
Gd(3)-O(38)	2.354(12)	Gd(5)-O(3)	2.372(10)
Gd(3)-O(35)	2.318(12)	Gd(5)-O(27)	2.367(11)
Gd(3)-O(34)	2.467(12)	Gd(5)-O(2)	2.365(11)
Gd(3)-O(29)	2.353(13)	Gd(5)-O(1A)	2.372(11)
Gd(3)-O(28)	2.377(11)	Gd(5)-N(12)#1	2.617(6)
Gd(3)-O(25)	2.360(12)	Gd(1)-O(8)	2.338(11)
Gd(3)-O(16)	2.348(13)	Gd(1)-O(4)	2.340(12)
Gd(3)-N(9)	2.620(7)	Gd(1)-O(31)	2.475(11)
Gd(2)-O(5)	2.335(11)	Gd(1)-O(24)	2.368(10)
Gd(2)-O(40)	2.358(13)	Gd(1)-O(17)	2.381(13)
Gd(2)-O(36)	2.369(14)	Gd(1)-O(15)	2.350(11)
Gd(2)-O(26)	2.431(10)	Gd(1)-N(11)	2.627(6)
Gd(2)-O(22)	2.378(12)	O(6)-N(3)	1.255(19)
Gd(2)-O(18)	2.479(11)	O(43)-N(5)	1.319(19)
Gd(2)-O(12)	2.319(12)	O(34)-N(8)	1.26(2)
Gd(2)-O(11)	2.341(11)	O(26)-N(7)	1.247(19)
Gd(4)-O(6)	2.462(11)	O(21)-N(10)	1.21(2)
Gd(4)-O(39)	2.331(12)	O(18)-N(4)	1.24(2)
Gd(4)-O(33)	2.369(14)	N(6)-O(30)	1.36(2)
Gd(4)-O(23)	2.346(11)	N(2)-O(31)	1.55(2)

Symmetry transformations used to generate equivalent atoms:

#1 x-1,y,z; #2 x+1,y,z; #3 x-1,y,z-1; #4 x+1,y,z+1

Table S2. Selected bond distances (Å) and for compound **2**.

2Tb			
Tb(2)-O(7)	2.345(6)	Tb(6)-O(21)	2.429(7)
Tb(2)-O(3)	2.331(7)	Tb(6)-O(30)	2.420(7)
Tb(2)-O(1)	2.318(7)	Tb(6)-O(32)	2.339(7)
Tb(2)-O(27)	2.358(7)	Tb(6)-O(41)	2.326(9)
Tb(2)-O(43)	2.468(7)	Tb(6)-O(14)	2.355(9)
Tb(2)-O(2)	2.336(7)	Tb(3)-N(1)#3	2.620(8)
Tb(2)-O(9)	2.348(7)	Tb(3)-O(33)	2.339(8)
Tb(2)-N(12)#1	2.606(8)	Tb(3)-O(10)	2.314(7)
Tb(1)-N(11)#2	2.594(8)	Tb(3)-O(23)	2.336(7)
Tb(1)-O(4)	2.337(7)	Tb(3)-O(6)	2.488(8)
Tb(1)-O(31)	2.497(7)	Tb(3)-O(19)	2.325(8)
Tb(1)-O(13)	2.328(7)	Tb(3)-O(20)	2.374(9)
Tb(1)-O(15)	2.367(7)	Tb(3)-O(39)	2.348(8)
Tb(1)-O(8)	2.342(7)	Tb(6)-O(40)	2.367(7)
Tb(1)-O(24)	2.334(6)	Tb(6)-O(36)	2.317(7)
Tb(1)-O(17)	2.344(6)	Tb(6)-O(26)	2.420(7)
Tb(4)-O(35)	2.336(7)	Tb(6)-O(18)	2.414(7)
Tb(4)-O(34)	2.464(7)	Tb(6)-O(12)	2.340(8)
Tb(4)-O(38)	2.345(8)	Tb(6)-O(11)	2.323(8)
Tb(4)-O(29)	2.362(8)	Tb(6)-O(44)	2.386(15)
Tb(4)-O(28)	2.369(8)	Tb(6)-O(22)	2.338(17)
Tb(4)-O(25)	2.320(7)	Tb(6)-O(22A)	2.386(18)
Tb(4)-O(16)	2.343(8)	Tb(6)-O(44A)	2.31(3)
Tb(4)-N(9)	2.574(9)	O(6)-N(3)	1.293(11)
Tb(5)-O(42)	2.317(6)	O(34)-N(8)	1.285(11)
Tb(5)-O(5)	2.325(7)	O(31)-N(2)	1.274(10)
Tb(5)-O(37)	2.363(7)	O(26)-N(7)	1.296(11)
N(6)-O(30)	1.283(11)	O(21)-N(10)	1.274(11)
N(5)-O(43)	1.300(10)	O(18)-N(4)	1.294(10)

Symmetry transformations used to generate equivalent atoms:

#1 x,y,z+1; #2 x+1,y,z-1; #3 x-1,y,z; #4 x+1,y,z; #5 x-1,y,z+1; #6 x,y,z-1

Table S3. SHAPE analyses for **1** and **2**.

	SAPR-8	TDD-8	BTPR-8		SAPR-8	TDD-8	BTPR-8
Gd1	1.335	**1.026**	2.043	Tb1	1.118	**1.089**	2.125
Gd6	1.183	**1.121**	2.099	Tb6	1.254	**1.094**	1.963
Gd4	1.832	**0.588**	2.422	Tb4	1.449	**0.862**	1.951
Gd2	2.529	**0.209**	2.297	Tb2	2.152	**0.629**	2.279
Gd3	1.553	**0.808**	1.967	Tb3	1.778	**0.524**	2.379
Gd5	1.913	**0.307**	2.161	Tb5	2.408	**0.245**	2.265

SAPR-8: Square antiprism; TDD-8: Triangular dodecahedron; BTPR-8: Biaugmented trigonal prism.

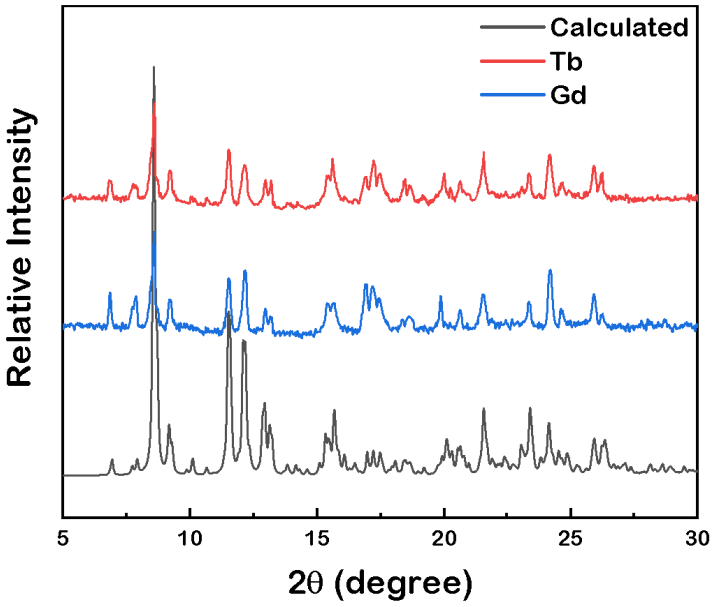

Figure S1 Powder X-ray diffraction patterns of complexes **1** and **2**.

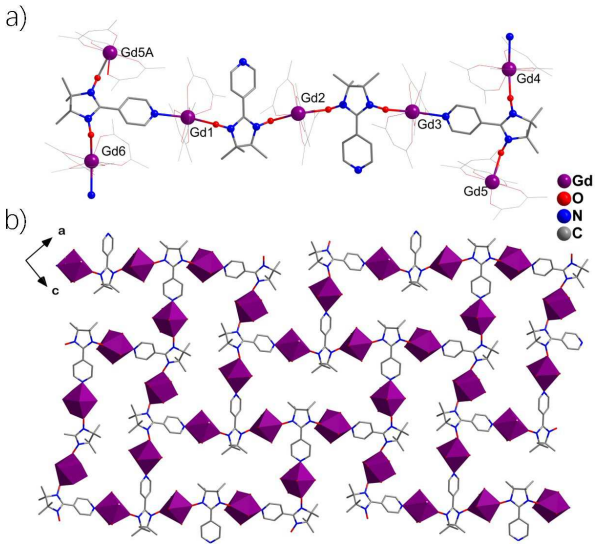

Figure S2 (a) The asymmetric unit (H and F atoms are omitted for clarity) and (b) the network structure of **1**.

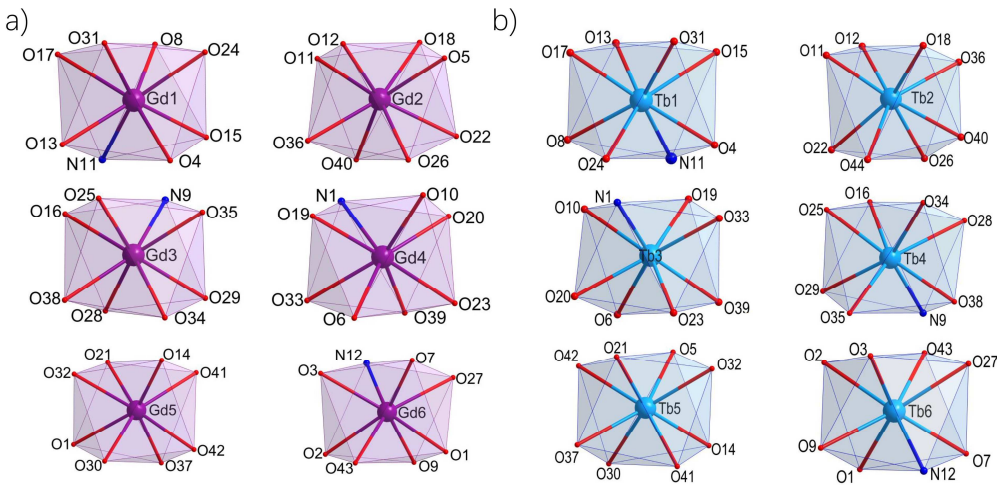

Figure S3 coordination polyhedron of all Gd^{III} centers in **1** and Tb^{III} centers in **2**.

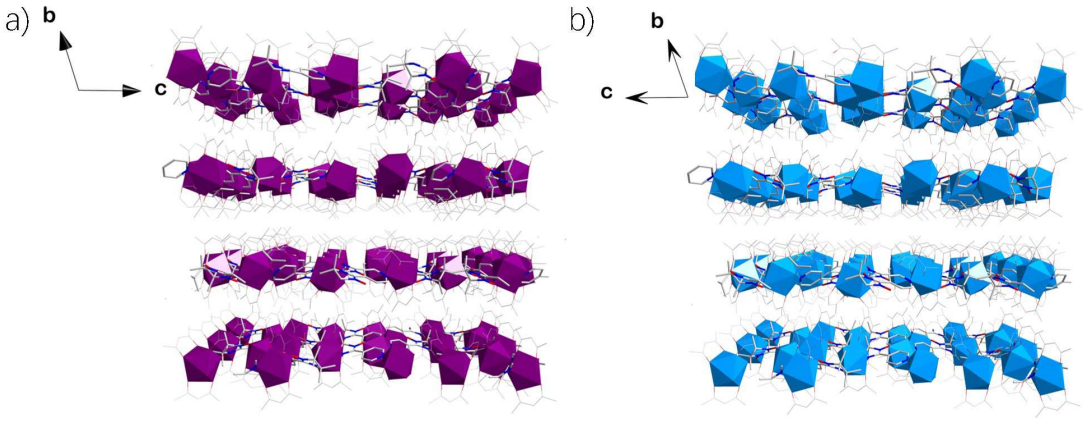

Figure S4 The packing diagram of (a) **1** and (b) **2**. (H and F atoms are omitted for clarity).

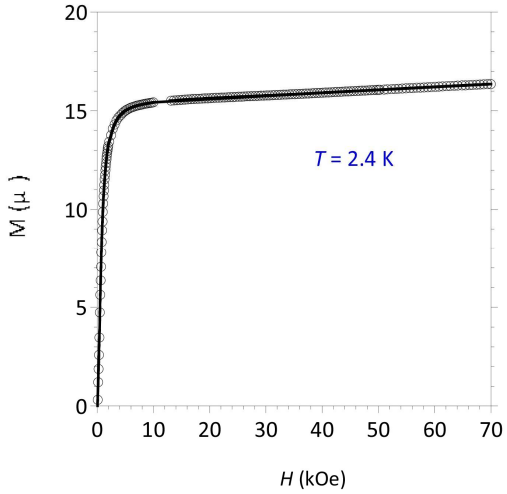

Figure. S5 M versus H of **2**.

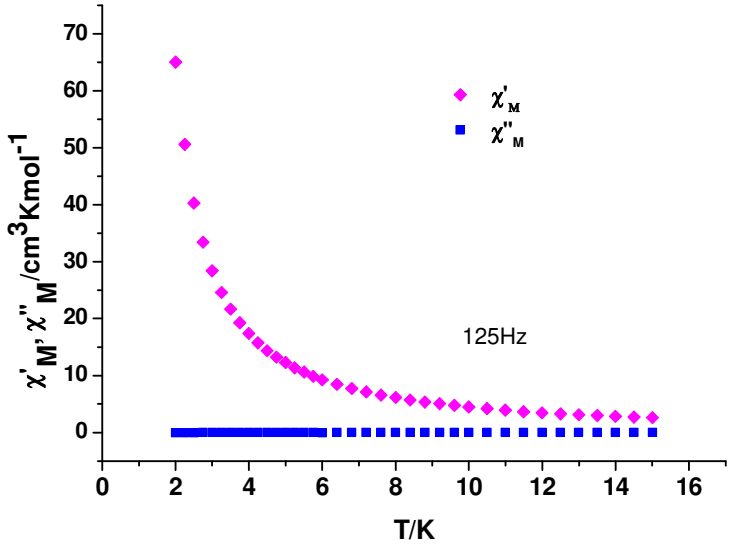

Figure S6 χ' and χ'' versus T plots under 0 dc field for **1**.

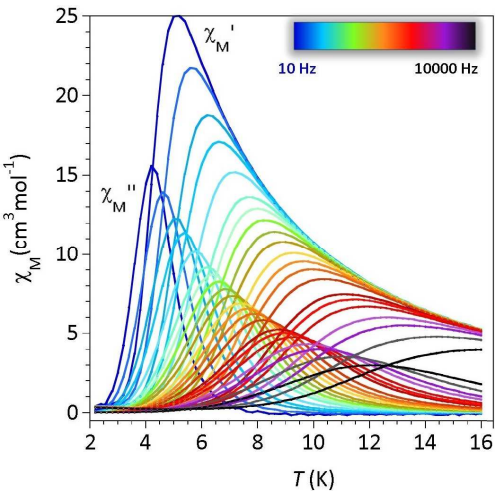

Figure S7. Complex **2**: χ' and χ'' versus T behaviors in 0 dc field for test frequencies from 10 to 10000 Hz

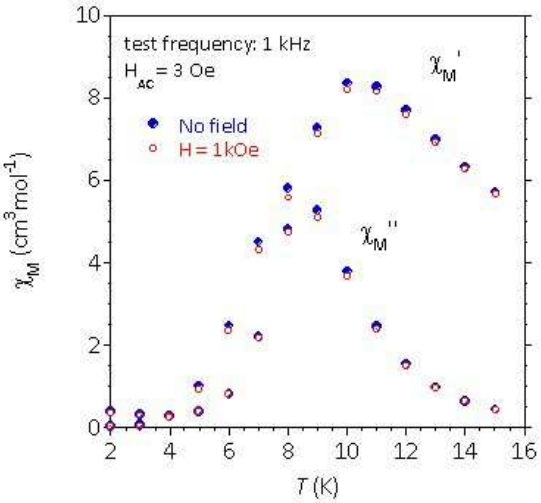

Figure S8. Measured χ' and χ'' versus T plots for **2** under 0 (in blue) and 1kOe (in red) dc field.

Table S4. Structure and magnetic parameters for Tb-NIT SMMs.

Complex	Structure	U_{eff}/K(H_{dc}/kOe)	τ_0 (s)	Ref.
$[Tb(hfac)_3(NITPhOEt)_2]$	Mononuclear	29.3	2.99×10^{-8}	1
$[Tb(hfac)_3(NIT2Py)]0.5C_7H_{16}$	Mononuclear	17.1	9.56×10^{-7}	2
$Tb(NITpic)_3$	Mononuclear	22.8	5.5×10^{-9}	3
$[Tb(tfa)_3(NITBzImH)]$	Mononuclear	13.95	4.56×10^{-7}	4
$[Tb(hfac)_3(NIT\text{-}Pyz)]$	Mononuclear	26	1.38×10^{-7}	5
$[Tb(hfac)_3(4\text{-}Me\text{-}3\text{-}NITtrz)(H_2O)]$	Mononuclear	16(3.0)	6.7×10^{-8}	6
[Tb(hfac)3(NITPhCOOMe)2]	Mononuclear	20(1.5)	1.94×10^{-8}	7
$[Tb(hfac)_3((NITPhPO(OEt)_2)]_2$	Binuclear	27.5(2.0)	2.64×10^{-9}	8
		21.0(2.0)	1.76×10^{-9}	
$[Tb(Phtfac)_3(NIT4Py)]_2$	Binuclear	22.8	4.1×10^{-8}	9
$[Tb(hfac)_3(NIT\text{-}5\text{-}Py\text{-}3Br)]_2$	Binuclear	28.7	5.9×10^{-9}	10
$[Tb(hfac)_3(NIT3Py)]_2$	Binuclear	19.0(3.0)	8.8×10^{-8}	11
$[Tb_3(hfac)_6(4\text{-}Me\text{-}3\text{-}NITtrz)_2(OH)_3]$	Trinuclear	14	3.1×10^{-7}	12
$Tb(acac)_3NIT2Py{\cdot}0.5H_2O$	Mononuclear	21.18(1.0)	1×10^{-7}	13
		26.0(3.5)	3×10^{-8}	
$[(Tb(hfac)_3)_6(NITPhOHexyl)_5(H_2O)_2]$	Hexanuclear	24.4	1.1×10^{-6}	14
		27.7	2.7×10^{-7}	
[Tb(hfac)3(NITPhCOOMe)]n	1D	36(1.0)	2.0×10^{-8}	15
$\{[Tb(tfa)_3]_3(NIT\text{-}4Py)_2\}$	2D	53.8	6.8×10^{-7}	this work

hfac = hexafluoroacetylacetonate; NITPhOEt = 4′-ethoxy-phenyl-4,4,5,5-tetramethylimidazoline-1-oxyl-3-oxide; NIT-2Py = 2-(2′-pyridyl)-4,4,5,5-tetramethylimidazoline-1-oxyl-3-oxide; NITpic = 2-(2′-pyridyl-3′-carboxyl)-4,4,5,5-tetramethylimidazoline-1-oxyl-3-oxide; tfa = trifluoroacetylacetonate; NIT-BzImH = 2-(2′-benzimidazolyl)-4,4,5,5-tetramethylimidazolyl-1-oxyl-3-oxide; NIT-Pyz = 2-{3-pyrazolyl}-4,4,5,5-tetramethylimidazoline-1-oxyl-3-oxide; 4-Me-3-NITtrz = 2-[3-(4-methyl-l,2,4-triazolyl)]-4,4,5,5-tetramethylimidazoline-1-oxyl-3-oxide; $NITPhPO(OEt)_2$ = 4′-[2-(1-oxyl-3-4,4,5,5-tetramethylimidazoline)-phenyl]diethoxylphosphine oxide; HPhtfac = 4,4,4-trifluoro-1-phenylbutane-1,3-dione; NITpPy = 2-(4-pyridyl)-4,4,5,5-tetramethyl-4,5-dihydro-1*H*-imidazolyl-1-oxyl-3-oxide; NIT-3Py = 2-(3-pyridyl)-4,4,5,5-tetramethylimidazoline-1-oxyl-3-oxide NIT-5-Br-3py = 2-(4,4,5,5-tetramethyl-3-oxylimidazoline-1-oxide)-5-bromo-3-pyridine; NITPhOHexyl = 2-(4-(hexyloxy)phenyl)-4,4,5,5-tetramethylimidazolin-1-oxyl-3-oxide); NITPhCOOMe = 2-(4-(methoxycarbonyl)phenyl)-4,4,5,5-tetramethylimidazolin-1-oxyl-3-oxide

References

(1) Zhou, N.; Ma, Y.; Wang, C.; Gong, F. X.; Tang, J.-K.; Xu, J.-X.; Yan, S.-P.; Cheng, P.; Li, L.-C.;Liao, D.-Z. A monometallic tri-spin single-molecule magnet based on rare earth radicals. *Dalton Trans.* **2009**, (40), 8489-8492.

(2) Wang, X.-L.; Li, L.-C.;Liao, D.-Z. Slow Magnetic Relaxation in Lanthanide Complexes with Chelating Nitronyl Nitroxide Radical. *Inorg. Chem.* **2010**, *49* (11), 4735-4737.

(3) Coronado, E.; Giménez-Saiz, C.; Recuenco, A.; Tarazón, A.; Romero, F. M.; Camón, A.;Luis, F. Single-Molecule Magnetic Behavior in a Neutral Terbium(III) Complex of a Picolinate-Based Nitronyl Nitroxide Free Radical. *Inorg. Chem.* **2011**, *50* (16), 7370-7372.

(4) Hu, P.; Zhu, M.; Mei, X.; Tian, H.; Ma, Y.; Li, L.;Liao, D. Single-molecule magnets based on rare earth complexes with chelating benzimidazole-substituted nitronyl nitroxide radicals. *Dalton Trans.* **2012**, *41* (48), 14651-14656.

(5) Chen, P. Y.; Wu, M. Z.; Liu, Z. Y.; Tian, L.;Zhang, Y. Q. Slow relaxation of the magnetization observed in mononuclear Ln–radical compounds with D_{4d} geometry configurations. *Dalton Trans.* **2019**, *48* (2), 558-565.

(6) Chen, P.-Y.; Wu, M.-Z.; Shi, X.-J.;Tian, L. A family of multi-spin rare-earth complexes based on a triazole nitronyl nitroxide radical: synthesis, structure and magnetic properties. *RSC Advances* **2018**, *8* (28), 15480-15486.

(7) Li, L-L; Liu, S.; Zhang, Y.; Shi, W.; Cheng, P. *Dalton Trans.,* **2015**, *44*(13), 6118-6125.

(8) Pointillart, F.; Bernot, K.; Poneti, G.;Sessoli, R. Crystal Packing Effects on the Magnetic Slow Relaxation of Tb(III)-Nitronyl Nitroxide Radical Cyclic Dinuclear Clusters. *Inorg. Chem.* **2012**, *51* (22), 12218-12229.

(9) Mei, X.-L.; Liu, R.-N.; Wang, C.; Yang, P.-P.; Li, L.-C.;Liao, D.-Z. Modulating spin dynamics of cyclic Ln^{III}-radical complexes (Ln^{III} = Tb, Dy) by using phenyltrifluoroacetylacetonate coligand. *Dalton Trans.* **2012**, *41*(10), 2904-2909.

(10) Xu, J.-X.; Ma, Y.; Liao, D.-z.; Xu, G.-F.; Tang, J.; Wang, C.; Zhou, N.; Yan, S.-P.; Cheng, P.;Li, L.-C. Four New Lanthanide-Nitronyl Nitroxide (Ln^{III} = Pr^{III}, Sm^{III},

Eu^{III}, Tm^{III}) Complexes and a Tb^{III} Complex Exhibiting Single-Molecule Magnet Behavior. *Inorg. Chem.* **2009**, *48* (18), 8890-8896.

(11) Tian, H.-X.; Liu, R.-N.; Wang, X.-L.; Yang, P.-P.; Li, Z.-X.; Li, L.-C.;Liao, D.-Z. Magnetic Slow Relaxation in Cyclic Tb^{III}-Nitronyl Nitroxide Radical Complexes. *Eur. J. Inorg. Chem.* **2009**, *2009* (29-30), 4498-4502.

(12) Shi, J.-Y.; Wu, M.-Z.; Chen, P.-Y.; Li, T.; Tian, L.;Zhang, Y.-Q. Terbium Triangle Bridged by a Triazole Nitronyl Nitroxide Radical with Single-Molecule-Magnet Behavior. *Inorg. Chem.* **2019**, *58* (21), 14285-14288.

(13) Lannes, A.; Intissar, M.; Suffren, Y.; Reber, C.;Luneau, D. Terbium(III) and Yttrium(III) Complexes with Pyridine-Substituted Nitronyl Nitroxide Radical and Different β-Diketonate Ligands. Crystal Structures and Magnetic and Luminescence Properties. *Inorg. Chem.* **2014**, *53* (18), 9548-9560.

(14) Houard, F.; Gendron, F.; Suffren, Y.; Guizouarn, T.; Dorcet, V.; Calvez, G.; Daiguebonne, C.; Guillou, O.; Le Guennic, B.; Mannini, M.;Bernot, K. Single-chain magnet behavior in a finite linear hexanuclear molecule. *Chem. Sci* **2021**, *12* (31), 10613-10621.

(15) Li, L-L; Liu, S.; Li, H.; Shi, W.; Cheng, P. *Chem. Commun.,* **2015**, *51*(54), 10933--10936.